REFERENCES

1. S. Yamashita and K. Hotate, Multiwavelength erbium-doped fiber laser using intracavity etalon and cooled by liquid nitrogen, Electron Lett 32 (1996), 1298–1299.
2. H.L. An, X.Z. Lin, E.Y.B. Pun, and H.D. Liu, Multi-wavelength operation of an erbium-doped fiber ring laser using a dual-pass Mach-Zehnder comb filter, Opt Commun 169 (1999), 159–165.
3. J. Chow, G. Town, B. Eggleton, M. Ibsen, K. Sugden, and I. Bennion, Multiwavelength generation in an erbium-doped fiber laser using in-fiber comb filters, IEEE Photon Technol Lett 8 (1996), 60–62.
4. X. Shu, S. Jiang, and D. Huang, Fiber grating Sagnac loop and its multiwavelength-laser application, IEEE PhotonTechnol Lett PTL-12 (2000), 980–982.
5. D. Wei, T. Li, Y. Zhao, and S. Jian, Multiwavelength erbium-doped fiber ring lasers with overlap written fiber Bragg gratings, Opt Lett 25 (2000), 1150–1152.
6. J. Sun, J. Qiu, and D. Huang, Multiwavelength erbium-doped fiber lasers exploiting polarization hole burning, Opt Commun 182 (2000), 193–197.
7. X.P. Dong, S. Li, K.S. Chiang, M.N. Ng, and B.C.B. Chu, Multiwavelength erbium-doped fiber laser based on a high-birefringence fiber loop mirror, Electron Lett 36 (2000), 1609–1610.
8. A. Bellemare, M. Karasek, M. Rochette, S. LaRochelle, and M. Tetu, Room temperature multifrequency erbium-doped fiber lasers anchored on the ITU frequency grid, J Lightwave Technol 18 (2000), 825–831.
9. O. Graydon, W.H. Loh, R.I. Laming, and L. Dong, Triple-frequency operation of an Er-doped twin core fiber loop laser, IEEE Photon Technol Lett 8 (1996), 63–65.
10. S. Li, H. Ding, and K.T. Chan, Erbium-doped fiber lasers for dual wavelength operation, Electron Lett 33 (1997), 50–53.
11. J.M. Battiato, T.F. Morse, and R.K. Kostuk, Dual-wavelength common-cavity co doped fiber laser, IEEE Photon Technol Lett 9 (1997), 913–915.
12. S. Yamashita, K. Hsu, and W.H. Loh, Miniature erbium: ytterbium fiber Fabry-Perot multiwavelength lasers, IEEE Photon. Technol. Lett., vol. 3, no. 4, pp. 1058–1064, 1997.
13. A.J. Poustie and N. Finlayson, Multiwavelength fiber laser using a spatial mode beating filter Opt Lett 19 (1994), 716–718.
14. N. Park and P.F. Wysocki, 24-line multiwavelength operation of erbium-doped fiber-ring laser, IEEE Photon Technol Lett 8 (1996), 1459–1461.
15. D. Falquier, D. Lande, J.L. Wagener, M.J.F. Digonnet, and H.J. Shaw, Measurement and modeling of the output polarization of erbium-doped fiber lasers, Doped fiber devices and systems, SPIE 2289 (1994), 24–39.
16. B. Srinivasan, S. Gupta, and R.K. Jain, Polarization anisotropic gain behavior in elliptical-core rare-earth doped fibers, Doped fiber devices and systems, SPIE 2289 (1994), 51–54.
17. J.T. Lin and W.A. Gambling, Polarization effects in fiber lasers: Phenomena, theory and applications, Fiber laser sources and amplifiers II, Proc SPIE 1373 (1990), 42–53.
18. J.H. Cordero, V.A. Kozlov, A.L.G. Carter, and T.F. Morse, Polarization effects in a high birefringence elliptical fiber laser with a Bragg grating in a low birefringence fiber, Appl Opt 39 (2000), 972–977.
19. E. Eickhoff, Y. Yen, and R. Ulrich, Wavelength dependence of birefringence in single-mode fiber, Appl Opt 20 (1981), 3428–3435.
20. U. Ghera, N. Konforti, and M. Tur, Wavelength tenability in a Nd-doped fiber laser with an intracavity polarizer, IEEE Photon Technol Lett 4 (1992), 4–6.
21. N. Friedman, A. Eyal, and M. Tur, The use of the principle states of polarization to describe tenability in a fiber laser, IEEE J Quantum Electron QE-33 (1997), 642–648.
22. D.B. Mortimore, Fiber loop reflectors, J Lightwave Technol 6 (1988), 1217–1224.
23. T.A. Birks and P. Morkel, Jones calculus analysis of single-mode fiber Sagnac reflector, Appl Opt 27 (1988), 3107–3112.
24. A.R. Pratt, K.Fujii, and Y.Ozeki, Gain control in L-band EDFAs by monitoring backward traveling C-band ASE, IEEE Photon Technol Lett 12 (2000), 983–985. .
25. H. Ono, M. Yamada, T. Kanamori, S. Sudo, and Y. Ohishi, 1.58- μm band gain-flattened erbium-doped fiber amplifiers for WDM transmission systems, J Lightwave Technol 17 (1999), 490–496.

GREEN'S FUNCTIONS FOR VERTICAL CURRENT SOURCES EMBEDDED IN UNIFORM WAVEGUIDES OR CAVITIES FILLED WITH MULTILAYERED MEDIA

Piotr M. Słobodzian,[1] A. Alvarez-Melcón,[2] Tomasz M. Grzegorczyk,[3] and Fred E. Gardiol[4]
[1] Institute of Telecommunications and Acoustics
Wroclaw University of Technology
Wyb. Wyspiańskiego 27
50-370 Wrocław, Poland
[2] Technical University of Cartagena
Campus Muralla del Mar s/n
30202 Cartagena, Spain
[3] Center of Electromagnetic Theory and Applications
Research Laboratory of Electronics
Massachusetts Institute of Technology
77 Massachusetts Avenue
Cambridge, Masssachusetts 02139
[4] Laboratory of Electromagnetics and Acoustics
Swiss Federal Institute of Technology
LEMA-EPFL
Lausanne, CH-1015, Switzerland

Received 29 October 2001

ABSTRACT: *A modal series representation of spatial-domain electric field Green's functions for arbitrarily oriented electric current sources embedded in shielded multilayer media is presented. The Green's functions associated with planar excitations are briefly recalled, and the method to compute them is generalized to vertical current sources, yielding new components of the Green's function necessary for the analysis of vertical metallizations embedded in waveguides or cavities.*
 Microwave Opt Technol Lett 33: 186–191, 2002; Published online in Wiley InterScience (www.interscience.wiley.com). DOI 10.1002/mop.10272

Key words: *waveguide Green's function; integral equation technique; shielded microwave circuits; vertical interconnects*

1. Introduction

In a variety of applications involving shielded multilayer microwave circuits, it is necessary to take into consideration vertical metallizations such as via holes, shorting pins, or even slots and holes made in the lateral walls of the shielding enclosure. One of the most commonly used methods for the rigorous full-wave analysis of this kind of problem is the integral-equation technique (IE), which relates the fields or the potentials to current sources, not known *a priori*, and which is then solved numerically by the method of moments (MoM). In this approach, a key step is the determination of the suitable Green's functions of the structure, which stand for the kernel of the IE.

Numerous techniques for the determination of Green's functions for waveguides or cavities have been developed in the past. These include the method of series expansion of the source function of the wave equation over a complete set of vector wave functions [1–4], the spectral domain method (SDM) [5–8], the approach based on the principle of scattering superposition [1, 9], the method of image source expansion [10], and the method based on the transmission-line network analogy and the modal field

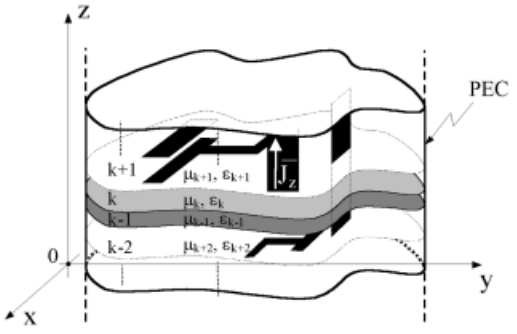

Figure 1 Vertical and horizontal metallizations embedded in a uniform waveguide filled with a multilayered medium

expansion [11, 12]. Most of these techniques, however, deal only with horizontal metallizations. Although some approaches have been derived for the treatment of vertical currents embedded in multilayered media of infinite transverse dimensions [13, 14], the same is generally not true when shielded structures are considered.

Consequently, the purpose of this article is to address this problem by generalizing the well-known electric-field integral-equation (EFIE) approach to the case of vertical current sources (i.e., z-axis directed in Figure 1) embedded in a uniform waveguide or cavity filled with a multilayered medium. The development uses a transmission-line network formalism for the longitudinal dependency of the electromagnetic field in conjunction with a modal field expansion in the space domain for the transverse dependency [15]. In order to demonstrate the applicability of the theory developed, a detailed treatment based on the EFIE-MoM technique of the problem of a vertical rectangular strip enclosed in a rectangular cavity is presented. Then, some aspects concerning the evaluation and computation of reaction integrals are discussed, because the way they are computed constitutes an important question in the development of efficient software codes. Finally, the input impedance of a rectangular strip embedded in a homogeneous rectangular cavity is computed. Because of the rotational symmetry of the problem, two methods have been implemented: one using the well-known Green's functions associated with horizontal excitations, and the other using the Green's functions associated with vertical excitations. The good agreement observed between the two approaches validates the newly developed vertical components.

2. Formulation of the problem

To analyze the problem of vertical metallizations involved in shielded multilayer microwave circuits, consider an infinite waveguide with perfect conducting walls, uniform along the z-axis, and filled with a layered medium as illustrated in Figure 1. Each layer is homogenous and possibly stratified so that the medium can be assumed to be uniaxially anisotropic. Hence, the Green's functions of the problem can be derived with the use of the transmission-line analogy applied along the z axis in conjunction with the modal field representation in the (xy) plane [15].

First Maxwell's equations are written for the fields in the kth layer of the medium (characterized by a permittivity ε_k and a permeability μ_k), taking into account the existence of both horizontal and vertical electric current sources. To do so, it is convenient to employ an invariant transverse vector formulation of Maxwell's field equations in the following form ($e^{j\omega t}$ time variation of the field is assumed and suppressed):

$$\frac{\partial \mathbf{H}_t^{(k)}}{\partial z} = \left(-j\omega\varepsilon_k + \frac{1}{j\omega\mu_k}\nabla_t\nabla_t\cdot\right)(\mathbf{i}_z \times \mathbf{E}_t^{(k)}) - \mathbf{i}_z \times \mathbf{J}_t, \tag{1a}$$

$$\frac{\partial \mathbf{E}_t^{(k)}}{\partial z} = \left(j\omega\mu_k - \frac{1}{j\omega\varepsilon_k}\nabla_t\nabla_t\cdot\right)(\mathbf{i}_z \times \mathbf{H}_t^{(k)}) - \frac{1}{j\omega\varepsilon_k}\nabla_t J_z, \tag{1b}$$

$$H_z^{(k)} = \frac{1}{j\omega\mu_k}\nabla_t\cdot(\mathbf{i}_z \times \mathbf{E}_t^{(k)}), \tag{1c}$$

$$E_z^{(k)} = -\frac{1}{j\omega\varepsilon_k}(\nabla_t\cdot(\mathbf{i}_z \times \mathbf{H}_t^{(k)}) + J_z), \tag{1d}$$

where the following transverse definitions have been used: $\mathbf{J}_t = \mathbf{i}_x J_x + \mathbf{i}_y J_y$, $\nabla_t = \mathbf{i}_x\,\partial/\partial x + \mathbf{i}_y\,\partial/\partial y$, $\mathbf{i}_x$ and $\mathbf{i}_y$being unitary vectors along $(0x)$ and (0y), respectively. Equations (1) show the separate dependencies of the fields on the transverse (x and y) and longitudinal coordinate z. It has been shown [15] that for a uniform infinite waveguide, the transverse dependency may be integrated out of equations (1a) and (1b) by means of vector modal functions $\mathbf{e}_i$ and $\mathbf{h}_i$ [of $E(\mathrm{TM}^z)$ and $H(\mathrm{TE}^z)$ type], which form an infinite complete set of orthogonal elements, in order to transform these equations into a set of transmission-line differential equations. To do this we need to express the transverse components of the electric and magnetic field in terms of the vector modal functions as:

$$\mathbf{E}_t^{(k)}(x,y,z) = \sum_i^\infty V_i^{\mathrm{TE}(k)}(z)\mathbf{e}_i^{\mathrm{TE}}(x,y) + \sum_i^\infty V_i^{\mathrm{TM}(k)}(z)\mathbf{e}_i^{\mathrm{TM}}(x,y), \tag{2a}$$

$$\mathbf{H}_t^{(k)}(x,y,z) = \sum_i^\infty I_i^{\mathrm{TE}(k)}(z)\mathbf{h}_i^{\mathrm{TE}}(x,y) + \sum_i^\infty I_i^{\mathrm{TM}(k)}(z)\mathbf{h}_i^{\mathrm{TM}}(x,y), \tag{2b}$$

where $V_i^{\mathrm{TE,TM}(k)}$, $I_i^{\mathrm{TE,TM}(k)}$ are the amplitude factors describing field changes along the z-axis. The substitution of Eq. (2) into (1a) and (1b) and integration of the resulting equation over the entire waveguide cross-section surface yields an infinite set of transmission-line differential equations, namely,

$$\frac{dV_i^{p(k)}(z)}{dz} = -j\beta_i^{(k)}Z_{C_i}^{p(k)}I_i^{p(k)}(z) + V_{g_i}^p,$$

$$\frac{dI_i^{p(k)}(z)}{dz} = -j\beta_i^{(k)}\frac{1}{Z_{C_i}^{p(k)}}V_i^{p(k)}(z) + I_{g_i}^p, \tag{3}$$

where $\beta_i^{(k)}$ is the propagation constant along the waveguide for the ith mode, $Z_{Ci}^{p(k)}$ is the modal characteristic impedance, p is the mode type (TE or TM), and $V_{g_i}^p$, $I_{g_i}^p$ are the voltage and current sources exciting the equivalent circuits of the medium, respectively. The latter are of the following form

$$V_{g_i}^p = -\frac{1}{j\omega\varepsilon_k}J_{mz_i}^p, \tag{4a}$$

$$I_{g_i}^p = -J_{mt_i}^p \tag{4b}$$

where $J_{mz_i}^p$ and $J_{mt_i}^p$ stand for amplitude factors in the modal expansion of the sources $\mathbf{J}_t$ and $\mathbf{i}_z J_z$. . The field representation given by Eqs. (2) and (3) provides a general solution for the field equations

in uniform waveguides, when both transverse $\mathbf{J}_t$ and longitudinal $\mathbf{i}_z J_z$ sources are included in the analysis.

With the use of (1)–(4), electric- and magnetic-field dyadic Green's functions can be derived for a given problem. In order to do so, it suffices to calculate the amplitude factors J^p_{mzi} and J^p_{mti} and in Eqs. (4) for point current sources (i.e., sources of the form of Dirac−δ) and to use Eqs. (2) and (3) to obtain the expression sought. For a waveguide structure, the complete electric dyadic Green's function due to electric current sources is given as follows (outside the source region):

$$G_{EJ}^{ss'(k)} = \sum_{i}^{\infty} \sum_{p=\mathrm{TE,TM}} V_i^{p(k)}(z, z') e_{s_i}^p(x, y) e_{s_i}^p(x', y'),$$

$$G_{EJ}^{zs'(k)} = \sum_{i}^{\infty} \sum_{p=\mathrm{TE,TM}} I_i^{p(k)}(z, z') A_i^p(x, y) e_{s_i}^p(x', y'), \tag{5a}$$

$$G_{EJ}^{sz(k)} = \sum_{i}^{\infty} \sum_{p=\mathrm{TE,TM}} V_i^{p(k)}(z, z') e_{s_i}^p(x', y') A'^p_i(x, y),$$

$$G_{EJ}^{zz(k)} = \sum_{i}^{\infty} \sum_{p=\mathrm{TE,TM}} I_i^{p(k)}(z, z') A_i^p(x, y) A'^p_i(x', y'), \tag{5b}$$

where $s \in \{x, y\}$, $s' \in \{x, y\}$ and where p is the mode type (TM^z or TE^z), i denotes (for a rectangular waveguide geometry) a double index mn of a double infinite summation, and where

$$\mathbf{e}_i^p(x, y) = \mathbf{i}_x e_{x_i}^p(x, y) + \mathbf{i}_y e_{y_i}^p(x, y), \tag{6}$$

$$A'^p_i(x', y') = \frac{1}{j\omega\varepsilon'} \nabla'_t \cdot \mathbf{e}_i^p(x', y'), \tag{7a}$$

$$A_i^p(x, y) = \frac{1}{j\omega\varepsilon} \nabla_t \cdot \mathbf{e}_i^p(x, y). \tag{7b}$$

The components associated with horizontal excitations $G_{EJ}^{ws'(k)}$, where $w \in \{x,y,z\}$, are given here for the sake of completeness. Those associated with vertical excitations [see Eq. (5b)] have to the authors' knowledge never been derived in such form, and allow rigorous analysis of vertical excitations also, as will be demonstrated in Section3.

Notice that the same approach can be used to obtain the final expressions for the magnetic field dyadic Green's function due to electric current sources, as well as for both field dyadic Green's functions due to magnetic current sources.

3. Rectangular waveguide with vertical metallizations

The focus is now narrowed to the case of a rectangular waveguide filled with a homogenous medium (characterized by ε and μ), in which a vertical metallization is embedded. For the sake of simplicity, the metallization is supposed to be of rectangular shape, lying in the (zy) plane, and sufficiently thin (e.g., a strip), so the current can be supposed to have only a vertical component $\mathbf{i}_z J_z$, as depicted in Figure 2.

With the use of an EFIE-MoM formulation [10], the generic expression of a MoM matrix element is

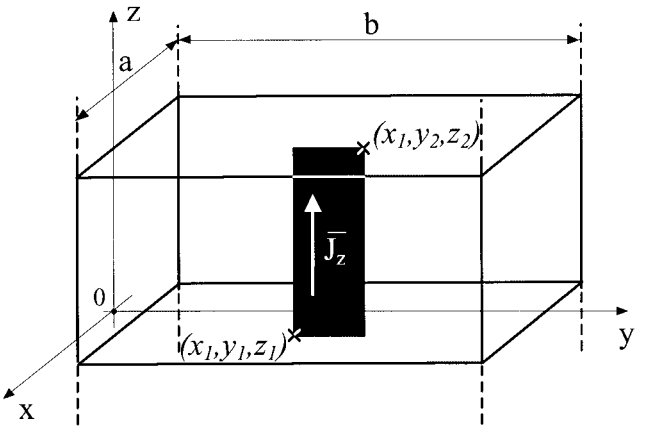

Figure 2 Vertical rectangular metallization in a uniform rectangular waveguide

$$Z_{zz}(k, j) = -\int\!\!\int_{S_k} \int\!\!\int_{S_j} G_{EJ}^{zz}(x, y, z, x', y', z') \cdot f_j(z') \cdot f_k(z)\, dS_j\, dS_k \tag{8}$$

where $f_j(z')$ and $f_k(z)$ and are the basis and testing functions, respectively, and dS_i is the surface over which $f_i(z)$ is defined. To evaluate integral (8), for the vector modal functions $\mathbf{e}_i$ and $\mathbf{h}_i$ and are needed in order to get an explicit formula for G_{EJ}^{zz}. For a simple waveguide geometry, such as rectangular, circular, elliptical, et cetera, the set of vector modal functions is known analytically [15, 16]. In the case of a rectangular geometry, the vertical component G_{EJ}^{zz} of the dyadic Green's function can be obtained as follows:

$$G_{EJ}^{zz} = -\sum_{m}^{\infty} \sum_{n}^{\infty} C_{mn}^{\mathrm{TM}}(z, z') \sin(k_{x_m} x) \sin(k_{y_n} y) \sin(k_{x_m} x') \sin(k_{y_n} y'), \tag{9}$$

where $m,n = 1, 2, 3, \ldots$ and the coefficient C_{mn}^{TM} in the expansion is given by

$$C_{mn}^{\mathrm{TM}}(z, z') = \frac{4}{j\omega\varepsilon ab}\left[-\frac{I_{mn}^{\mathrm{TM}}(z, z')}{j\omega\varepsilon'} k_{\rho_{mn}}^2 + \delta(z, z')\right], \tag{10}$$

where $I_{mn}^{\mathrm{TM}}(z, z')$ is the current in the equivalent transmission line excited by the voltage source $V_g = 1\mathrm{V}$ as shown in Figure 3, $k_{\rho_{mn}}$ is the transverse cutoff wave number, a and b are the waveguide dimensions (see Figure 2), and ε and ε' are the permittivities taken at the point of observation and source, respectively (in the present case $\varepsilon=\varepsilon'$ because there is a single homogenous layer). As can be seen in Eq. (9), G_{EJ}^{zz} is expressed as an infinite sum of TM^z modes only, which is justified by the fact that vertical electric current sources do not excite the vertical component of the magnetic field, so that TE^z modes can not exist in this case (see also e.g. [17]).

The next step is to calculate the elements of the MoM matrix. If Eq (9) is substituted for (8) and the rectangular rooftop basis functions definitions for $f_i(z)$, are used, one can derive an equation for the reaction integral Ir_{mn} of the following form:

$$Ir_{mn}(k, j) = \int_{\partial z_k} f_k(z) \int_{\partial z_j} I_{mn}^{\mathrm{TM}}(z, z') f_j(z')\, dz'\, dz, \tag{11}$$

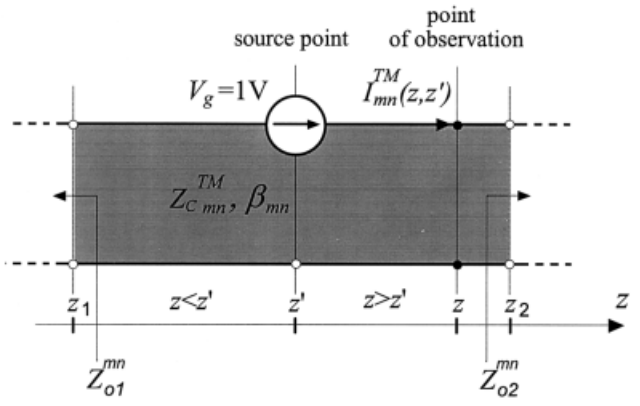

Figure 3 Equivalent transmission line model for a single layer (particularized to the modeling of G^{zz}_{EJ})

where ∂z_i is the linear domain over which the z dependency of f_i is defined.

Although $I^{\mathrm{TM}}_{mn}(z, z')$ appears as a function of both z and z', the double integral in Eq. (11) can be transformed into a product of two separated single integrals, so that the calculations can then be carried out more efficiently. The separation is possible and in addition, the calculations are numerically more stable if the current in the transmission line is expressed in terms of exponential functions as follows:

$$I^{\mathrm{TM}}_{mn}(z, z') = D^{\mathrm{TM}}_{mn} \cdot \{e^{j\beta_{mnz'}} e^{j\beta_{mnz}} + C^{mn}_1 e^{-j\beta_{mnz'}} e^{-j\beta_{mnz}} + C^{mn}_2 e^{j\beta_{mn}|z-z'|} + C^{mn}_3 e^{-j\beta_{mn}|z-z'|}\}. \quad (12)$$

For a single-layer medium, coefficients D, C_1, C_2 and C_3 do not depend on the position of the source and observer, so that they can be expressed as:

$$D^{\mathrm{TM}}_{mn} = \frac{1}{2Z^{\mathrm{TM}}_{C_{mn}} \cdot (T^{mn}_{o1} - T^{mn}_{o2})}, \quad (13a)$$

$$C^{mn}_1 = T^{mn}_{o1} T^{mn}_{o2}, \quad (13b)$$

$$C^{mn}_2 = -T^{mn}_{o1}, \quad (13c)$$

$$C^{mn}_3 = -T^{mn}_{o2}, \quad (13d)$$

where

$$T^{mn}_{o1} = \frac{Z^{mn}_{o1} - Z^{\mathrm{TM}}_{C_{mn}}}{Z^{mn}_{o1} + Z^{\mathrm{TM}}_{C_{mn}}} \cdot e^{j\beta_{mn}2z_1}, \quad (14a)$$

$$T^{mn}_{o2} = \frac{Z^{mn}_{o2} + Z^{\mathrm{TM}}_{C_{mn}}}{Z^{mn}_{o2} - Z^{\mathrm{TM}}_{C_{mn}}} \cdot e^{j\beta_{mn}2z_2}, \quad (14b)$$

where Z^{mn}_{o1} and Z^{mn}_{o2} are the impedances at the boundaries z_1 and z_2 of the layer, respectively, and $Z^{\mathrm{TM}}_{C_{mn}}$ is the modal characteristic impedance of the equivalent transmission-line model, as shown in Figure 3.

Equations (11)–(14) constitute the final solution to the problem of a vertical rectangular strip embedded in a uniform rectangular waveguide or cavity filled with homogeneous stratified medium. With the use of the approach presented in this section one is now able to rigorously analyze vertical metallizations involved in shielded multilayer microwave circuits.

4. Example

In order to validate the solution derived in the previous section, two simple problems will be analyzed, namely, a horizontal and a vertical rectangular strip embedded in a cavity (a rectangular waveguide short-circuited at the ends), as shown in Figure 4. Assume, for the sake of simplicity, that the strip extends between two walls of the cavity. The two apparently different problems, depicted in Figures 4(a) and 4(b), respectively, are in fact identical, since a simple axis rotation allows passing from one to the other. However, these two problems will be analyzed in two different ways: with the well-known horizontal Green's functions [see Eqs. (5a)] [11, 12], for the case of Figure 4(a), and with the newly

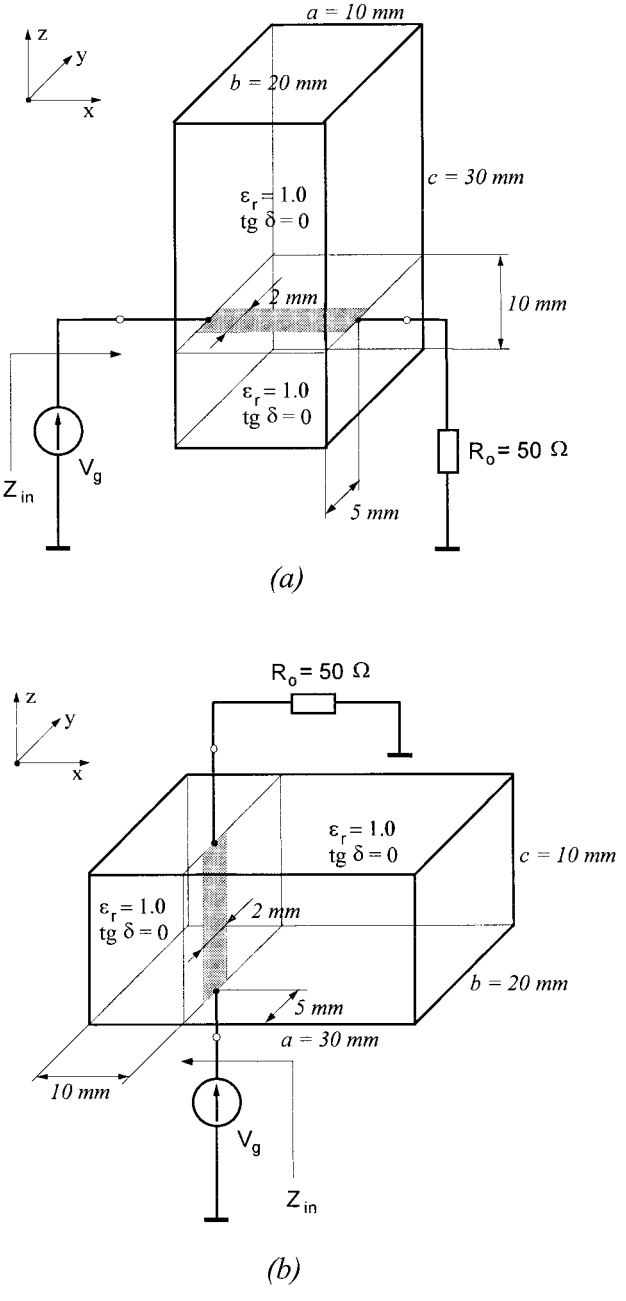

Figure 4 (a) Horizontal and (b) vertical strip embedded in a rectangular cavity

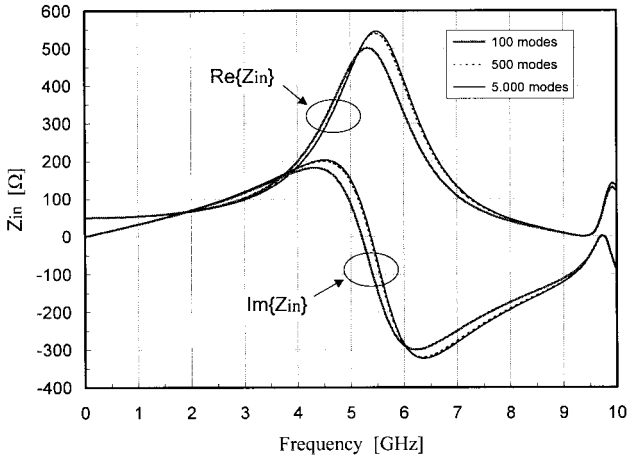

Figure 5 Input impedance of the horizontal strip shown in Figure 4(a)

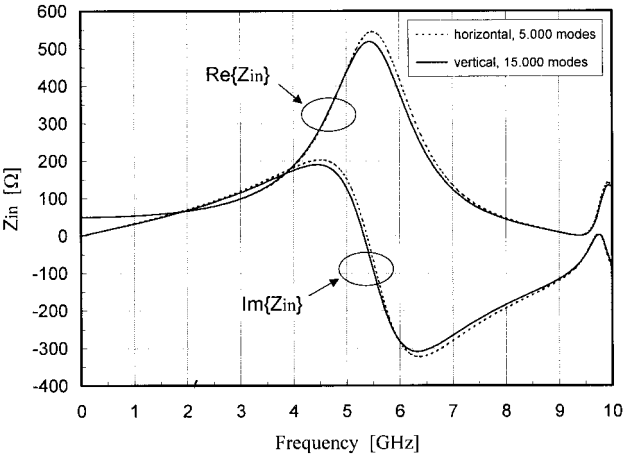

Figure 7 Input impedance: comparison between the results obtained with the use of horizontal and vertical Green's functions

derived vertical Green's functions [see Eq. (5b)], for the case of Figure 4(b).

In order to compare the solutions given by the two methods, the input impedance of the strip has been computed. In addition, in order to investigate the convergence of the solutions, the computations have been performed with a different number of vector modal functions used in the evaluation of the Green's functions. Convergence results for the first method are shown in Figure 5, while those for the second method are shown in Figure 6. Observe that when horizontal Green's functions are used, the convergence is faster and it suffices to take about 500 modes to get stable and accurate results. The method using vertical Green's functions, on the other hand, exhibits slower convergence properties as compared to the previous one. Although the solution eventually tends to the correct value, about 10^4 modes need to be taken into account in order to achieve stable results. It has also been observed that this convergence is better for a similar problem, but with a lossy medium and higher dielectric constant, for which good convergence properties were observed with about 5000 modes already. Finally, Figure 7 presents a comparison of the input impedances obtained with the two methods, and shows a very good agreement between them, therefore validating the new vertical components derived.

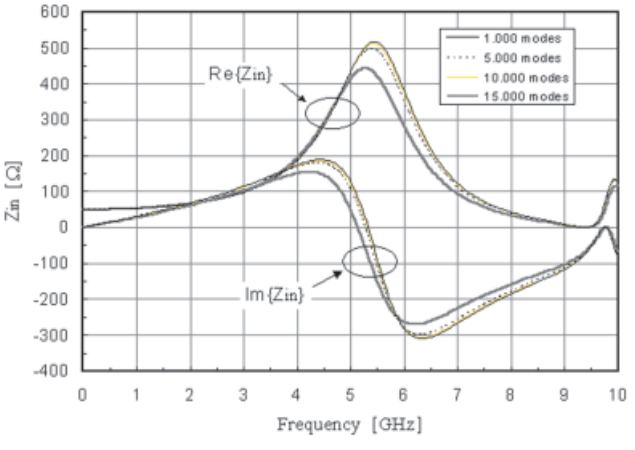

Figure 6 Input impedance of the vertical strip shown in Figure 4(b). [Color figure can be viewed in the online issue, which is available at www.interscience.wiley.com.]

It is also worth mentioning that special attention must be paid to the evaluation of certain exponential functions, because otherwise numerical underflow or overflow can occur during the computation. For example, a direct implementation of Eqs. (11)–(14) can result in numerical instabilities just above 100–200 modes. However, careful control of these instabilities allows the building of efficient software codes, and accurate results can be obtained even with more than 10^4 modes, as demonstrated in the example presented in this article.

5. Conclusions

A general theory of the dyadic Green's function for vertical and horizontal electric current sources radiating in uniform waveguides has been presented. A precise treatment, based on the integral equation formulation of vertical rectangular metallizations embedded in uniform rectangular waveguides or cavities filled with multilayer media has been proposed. Finally, a simple example of a vertical rectangular strip embedded in a rectangular cavity has been analyzed in order to validate the method proposed. The good agreement between results obtained by horizontal and vertical Green's functions approaches has confirmed the validity of the latter.

In spite of the slower convergence rate of the approach proposed, its availability presents numerous advantages, because now the solution to the problem of horizontal and vertical metallizations can be combined into a single algorithm. Therefore, the gain obtained with the formulation presented is the capability of accurately analyzing shielded MMICs containing via holes and vertical interconnections between horizontal metallizations of different layers.

Dr. Piotr Slobodzian expresses his sincere gratitude and acknowledgement to Professor Fred E. Gardiol who invited him at LEMA-EPFL, Lausanne, Switzerland and helped him to obtain a scholarship granted by the *Swiss Federal Scholarship Commission*.

REFERENCES

1. C. T. Tai, Dyadic Green's functions in electromagnetic theory, 2nd ed., IEEE Press Series on Electromagnetic Waves, New York, 1993.
2. Y. Rahmat-Samii, On the question of the dyadic Green's function at the source region in waveguides and cavities, IEEE Trans Microwave Theory Tech MTT-23 (1975), 762–765.
3. B. Gnilenko and A.B. Yakovlev, Electric dyadic Green's functions for

application to shielded multilayered transmission line problems, IEE Proc Microwave Antennas Propagat146 (1999).
4. L.P. Dunleavy and P.B. Katehi, A generalised method for analysing shielded thin microstrip discontinuities, IEEE Trans Microwave Theory Tech MTT-36 (1988), 1758–1766.
5. J.C. Rautio and R.F. Harrington, An electromagnetic time-harmonic analysis of shielded microstrip circuits, IEEE Trans Microwave Theory Tech MTT-35 (1987), 726–730.
6. A. Hill and V.K. Tripathi, An efficient algorithm for the three-dimensional analysis of passive microstrip components and discontinuities for microwave and millimeter-wave integrated circuits, IEEE Trans Microwave Theory Tech MTT-39 (1991), 83–91.
7. J. Railton and S.A. Meade, Fast rigorous analysis of shielded planar filters, IEEE Trans Microwave Theory Tech MTT-40 (1992), 978–985.
8. J.Y. Lee, T.S. Horng, and N.G. Alexopoulos, Analysis of cavity-backed aperture antennas with a dielectric overlay, IEEE Trans Antennas Propagat AP-42 (1994), 1556–1562.
9. T.G. Livernois and P.B. Katehi, A generalized method for deriving the space-domain Green's function in a shielded, multilayer substrate structure with applications to MIS slow-wave transmission lines, IEEE Trans Microwave Theory Tech MTT-37 (1989), 1761–1767.
10. K.A. Michalski and J.R. Mosig, Multilayered media Green's functions in integral equation formulations, IEEE Trans Antennas Propagat AP-45 (1997), 508–519.
11. G.V. Eleftheriades, J.R. Mosig, and M. Guglielmi, A fast integral equation technique for shielded planar circuits defined on nonuniform meshes, IEEE Trans Microwave Theory Tech MTT-44 (1996), 2293–2296.
12. A. Alvarez-Melcón, M. Guglielmi, and J.R. Mosig, Efficient CAD of boxed microwave circuits based on arbitrary rectangular elements, IEEE Trans Microwave Theory Tech MTT-47 (1999), 1045–1058.
13. N. Kinayman and M.I. Aksun, Efficient use of closed-form Green's functions for the analysis of planar geometries with vertical connections, IEEE Trans Microwave Theory Tech MTT-45 (1997), 593–602.
14. T.M. Grzegorczyk and J.R. Mosig, Full-wave analysis of antennas containing horizontal and vertical metallizations embedded in multilayered media, IEEE Trans Antennas Propagat, in press.
15. N. Marcuwitz (ed.), Waveguide handbook, M.I.T. Radiation Laboratory Series, Boston: Boston Technical, 1964.
16. A. Balanis, Advanced engineering electromagnetics, New York: Wiley, 1989.
17. P. Bernardi and R. Cicchetti, Dyadic Green's function for conductor-backed layered structures excited by arbitrary tridimensional sources, IEEE Trans Microwave Theory Tech MTT-42 (1994), 1474–1483.

THEORETICAL INVESTIGATIONS INTO BINOMIAL DISTRIBUTIONS OF PHOTONIC BANDGAPS IN MICROSTRIPLINE STRUCTURES

Nemai C. Karmakar
School of Electrical and Electronic Engineering
Nanyang Technological University
Nanyang Avenue
Singapore 639697

Received 22 October 2001

ABSTRACT: *Conventional circular patterned microstrip PBGs have constraints in broad stop-band response due to high ripple heights in S parameters. In this Letter, a novel configuration with the nonuniform dimensions of circular-patterned PBGs to improve the rejection bandwidth and the ripples is proposed. The dimensions of the circles are varied proportionally to the amplitude coefficients of the binomial distribution. The S-parameter versus frequency plot of a 10-element binomially distributed circular-patterned PBG array has been presented. The result reveals that the binomial distribution improves the performance by suppressing ripples and generating distinct stop-band and low-pass responses and sharp cutoffs. A tandem of two such PBG lines yields even wider and distinct stop-band and low-pass responses.* © 2002 Wiley Periodicals, Inc. Microwave Opt Technol Lett 33: 191–196, 2002; Published online in Wiley InterScience (www.interscience.wiley.com). DOI 10.1002/mop.10273

Key words: *microstrip lines; photonic bandgap; annular ring PBG; ripples; stop band; filters; binomial distribution*

1. INTRODUCTION

Recent years have witnessed technological innovations in material sciences and processing techniques. There has been growing interest in the development of artificial materials that yield extraordinary performances for devices in microwave and millimeter-wave frequencies. Photonic crystals are such artificial materials. They are made of 2D and 3D periodic dielectrics, in analogy to crystals made of periodic atoms or molecules that exhibit electron bandgap. At microwave frequencies electromagnetic waves behave in photonic substrates as electrons behave in semiconductors. PBG materials are periodic structuresthat exhibit wide bandpass and band-rejection properties at microwave and millimeter-wave frequencies. Introducing periodic perturbations such as dielectric rods, holes, and patterns in waveguides and microstrip substrates forms PBG materials. Although various configurations have been proposed in the literature, only the planar etched PBG configurations [1–5] have attracted much interest because of their ease of fabrication with photolithographic MIC, MMIC, and MEMS processes. The electromagnetic waves in a PBG material are impeded due to the periodic discontinuity, hence making a slow-wave structure. In a slow-wave structure, the effective wavelength increases without any dimensional changes, hence compact design is achieved.

Surface-wave propagation in microstrip dielectric materials is a serious problem. Surface waves reduce efficiency and gain, limit bandwidth for active and passive microwave devices, and increase end-fire radiation and cross-polarization levels in antennas. PBG-engineered materials suppress surface waves [6, 11] in dielectric slabs. Consequently, the performances of active and passive microwave components are enhanced. The unique properties of PBG materials in microwave and millimeter-wave frequencies make them excellent platforms for planar transmission lines; waveguides; power combiners/dividers; filters; diplexers; EMC measurements; broadband absorbers and reflectors; high-efficiency broadband power amplifiers; phased arrays; highly directive, high efficiency, and broadband antenna elements; and many other devices. The research is continuing to explore the full benefit of the photonic bandgap materials for microwave and millimeter-wave applications [5–12].

The behavior of PBG-engineered materials can be controlled with the proper choice of different lattice structures and lattice parameters, such as the filling factor, the patterns/geometries of perturbations, and the distributions of PBG patterns. Lopeteg et al. [4] report sinusoidal and triangular patterns along with the conventional circular pattern. Laso et al. [3] describe a nonuniform distribution and the tapered radii of circular PBG patterns with Gaussian distribution and chirped periods. Lopetag et al. [5] report a tapered distribution of a circular-patterned PBG based on the Hamming window. Yun and Chang [13] describe uniplanar 1D PBG structures and resonators on coplanar waveguides, slot lines, and coplanar striplines. Different resonator lines with PBG reflec-